Chiral *g*-matrix folding-model approach to reaction cross sections for scattering of Ca isotopes on a C target

Shingo Tagami [1], Masaomi Tanaka [1], Maya Takechi,[2] Mitsunori Fukuda,[3] and Masanobu Yahiro [1,*]

[1]*Department of Physics, Kyushu University, Fukuoka 812-8581, Japan*
[2]*Niigata University, Niigata 950-2181, Japan*
[3]*Department of Physics, Osaka University, Osaka 560-0043, Japan*

We first predict the ground-state properties of Ca isotopes using the Gogny-D1S Hartree-Fock-Bogoliubov with and without the angular momentum projection. We find that ^{64}Ca is an even-dripline nucleus and ^{59}Ca is an odd-dripline nucleus, using A dependence of the one-neutron separation energy S_1 and the two-neutron separation energy, S_2. As for S_1, S_2 and the binding energies E_B, our results agree with the experimental data in $^{40-58}$Ca. As other ground-state properties of $^{40-60,62,64}$Ca, we predict charge, proton, neutron, matter radii, neutron skin, and deformation. As for charge radii, our results are consistent with the experimental data in $^{40-52}$Ca. For ^{48}Ca, our results on proton, neutron, matter radii agree with the experimental data. Recently, Tanaka *et al.* measured interaction cross sections for $^{42-51}$Ca scattering on a ^{12}C target at an incident energy per nucleon of $E_{\rm lab} = 280$ MeV. Second, we predict reaction cross sections σ_R for $^{40-60,62,64}$Ca using a chiral *g*-matrix double-folding model (DFM). To show the reliability of the present DFM for σ_R, we apply the DFM for the data on ^{12}C scattering on ^{9}Be, ^{12}C, ^{27}Al targets in $30 \lesssim E_{\rm lab} \lesssim 400$ MeV and show that the present DFM is good in $30 \lesssim E_{\rm lab} \lesssim 100$ MeV and $250 \lesssim E_{\rm lab} \lesssim 400$ MeV. For $110 \lesssim E_{\rm lab} \lesssim 240$ MeV, our results have small errors. To improve the present DFM for σ_R, we propose two prescriptions.

I. INTRODUCTION

Systematic understanding of unstable nuclei is a goal in nuclear physics. In fact, neutron-rich nuclei near the neutron dripline are synthesized in nature by the r process. In particular, the binding energies E_B affect the synthesis; see the homepage NuDat 2.7 [1] for the measured values. The odd and the even dripline are determined from mass-number (A) dependence of the one-neutron separation energy $S_1(A) \equiv E_B(A) - E_B(A - 1)$ and the two-neutron separation energy $S_2(A) \equiv E_B(A) - E_B(A - 2)$; see Refs. [1–4] for the experimental data.

In many papers using the Glauber model, nuclear matter radii r_m are extracted from interaction cross sections σ_I and reaction cross sections σ_R ($\sigma_R \approx \sigma_I$); see Refs. [5–12] as important papers. Particularly for halo nuclei, the r_m are determined for ^{6}He, ^{8}B, ^{11}Li, and ^{11}Be in Refs. [5,6]; ^{19}C in Ref. [9]; ^{22}C in Refs. [10,11]; and ^{37}Mg in Ref. [12]. We proposed a parameter quantifying the halo nature of one-neutron nuclei [13]; see Fig. 3 of Ref. [13] for seeing how halo the nucleus is.

High-precision measurements of σ_R within 2% error were made for ^{12}C scattering on ^{9}Be, ^{12}C, and ^{27}Al targets in a wide range of incident energies [7]; say, $30 \lesssim E_{\rm lab} \lesssim 400$ MeV for $E_{\rm lab}$ being the incident energy per nucleon. In fact, the r_m of ^{9}Be, ^{12}C, and ^{27}Al were determined by the

Glauber model. Recently, in RIKEN, Tanaka *et al.* measured σ_I for $^{42-51}$Ca scattering on a ^{12}C target at $E_{\rm lab} = 280$ MeV [14].

The reliability of the Glauber model was investigated by constructing the multiple scattering theory for nucleus-nucleus scattering [15]. The eikonal approximation used in the Glauber model is not good for nucleon-nucleon collision in nucleus-nucleus scattering; see Fig. 1 of Ref. [15]. This problem can be solved by formulating the Glauber model with the multiple scattering theory. The formulation shows that the nucleon-nucleon collision should be described by the *g* matrix for lower energies and by the *t* matrix for higher energies. The Glauber model is thus justified for higher $E_{\rm lab}$, say, in $E_{\rm lab} \gtrsim 150$ MeV.

The *g*-matrix double-folding model (DFM) [16–23] is a standard way of deriving microscopic optical potentials of nucleus-nucleus elastic scattering. The *g*-matrix DFM is thus a standard method for calculating σ_R. The microscopic potentials are obtained by folding the *g* matrix with projectile and target densities. In fact, the potentials have been used for elastic scattering in many papers. Using the DFM with the Melbourne *g* matrix, we discovered that ^{31}Ne is a halo nucleus with strong deformation [19] and determined, with high accuracy, the r_m for Ne isotopes [20] and for Mg isotopes [22].

As for the symmetric nuclear matter, Kohno calculated the *g* matrix by using the Brueckner-Hartree-Fock (BHF) method with chiral N^{3}LO 2NFs and NNLO 3NFs [24]. The BHF energy per nucleon becomes minimum at $\rho = 0.8\rho_0$ for the cutoff scale $\Lambda = 550$ MeV [25] if the relation $c_D \simeq 4c_E$ is

*orion093g@gmail.com

satisfied, where ρ is nuclear matter density and ρ_0 stands for the normal density. He then took $c_D = -2.5$ and $c_E = 0.25$ so that the energy per nucleon may be minimum at $\rho = \rho_0$. Eventually, a better saturation curve was obtained. The framework is applied for positive energies. The resulting nonlocal chiral g matrix is localized into three-range Gaussian forms by using the localization method proposed by the Melbourne group [17,26,27]. We refer to the resulting local g matrix as Kyushu g matrix in this paper [23].

As an *ab initio* method for structure of Ca isotopes, we can consider the coupled-cluster method [28,29] with chiral interaction. Chiral interactions have been constructed by two groups [30–32]. Among the effective interactions, NNLO$_{\rm sat}$ [33] is the next-to-next-to-leading order chiral interaction that is constrained by radii and binding energies of selected nuclei up to $A \approx 25$ [29]. In fact, the *ab initio* calculations were done for Ca isotopes [29,33,34]. Garcia Ruiz *et al.* evaluated the charge radii $r_{\rm ch}$ for $^{40-54}$Ca [34], using the coupled-cluster method with two low-momentum effective interactions of Refs. [35,36], derived from the chiral interaction with the renormalization group method.

Particularly for a neutron-rich double-magic nucleus ^{48}Ca, the neutron skin $r_{\rm skin} = r_n - r_p$ was directly determined from a high-resolution measurement of $E1$ polarizability in RCNP [37], where r_n and r_p are the rms radii of neutron and proton distributions, respectively. The value $r_{\rm skin} = 0.14$–0.20 fm is important to determine not only the equation of state but also r_n and r_m of ^{48}Ca. Using $r_p = 3.40$ fm [38–40] evaluated from the electron scattering, we can find that $r_n = 3.54$–$3.60 = 3.57(3)$ fm and $r_m = 3.48$–$3.52 = 3.50(2)$ fm.

In this paper, we predict the ground-state properties of Ca isotopes using the Gogny-D1S Hartree-Fock-Bogoliubov (GHFB) with and without the angular momentum projection (AMP) [41] and predict σ_R for scattering of Ca isotopes on a ^{12}C target at $E_{\rm lab} = 280$ MeV by taking the Kyushu g-matrix DFM [23]. The GHFB with and without the AMP are referred to as "GHFB + AMP" and "GHFB," respectively. Details of our predictions are shown below.

As an essential property of Ca isotopes, we first determine the odd and even driplines for Ca isotopes by seeing A dependence of S_1 and S_2 and find that ^{64}Ca is an even-dripline nucleus and ^{59}Ca is an odd-dripline nucleus. As for E_B, S_1, S_2, our results agree with the experimental data for $^{40-58}$Ca [1–4]. Our results are thus accurate enough for the prediction on the odd and even driplines.

As other grand-state properties, we consider $r_{\rm ch}$, r_p, r_n, r_m, $r_{\rm skin}$, and deformation for $^{40-60,62,64}$Ca. As for the charge radii $r_{\rm ch}$, our results are consistent with the data [39] determined from the isotope shift method based on the electron scattering in $^{40-52}$Ca. As for r_p, r_n, r_m, and $r_{\rm skin}$, the experimental data are available for ^{48}Ca [37], and our results agree with the data. The success on the ground-state properties indicates that the densities calculated with GHFB and GHFB + AMP are reliable for Ca isotopes.

The Kyushu g-matrix folding model is successful in reproducing the differential cross sections of p scattering at $E_{\rm lab} = 65$ MeV [42] and of ^{4}He scattering at $E_{\rm lab} = 30$–200 MeV [23,43]. However, it is not clear whether the Kyushu g-matrix DFM is reliable for σ_R. In order to

investigate the reliability, we apply the Kyushu g-matrix DFM for measured σ_R on ^{12}C scattering from ^{9}Be, ^{12}C, and ^{27}Al targets in $30 \lesssim E_{\rm lab} \lesssim 400$ MeV and confirm that the present DFM is reliable in $30 \lesssim E_{\rm lab} \lesssim 100$ MeV and $250 \lesssim E_{\rm lab} \lesssim 400$ MeV. We then predict σ_R for scattering of Ca isotopes on a ^{12}C target at $E_{\rm lab} = 280$ MeV, using the Kyushu g-matrix DFM [23]. The reason for this prediction is that (1) the data on σ_R for $^{42-51}$Ca will be available soon and (2) the densities are determined accurately for Ca isotopes.

The present DFM is not accurate enough for ^{12}C - ^{12}C scattering in $110 \lesssim E_{\rm lab} \lesssim 240$ MeV. In order to improve the present DFM in $110 \lesssim E_{\rm lab} \lesssim 240$ MeV, we propose two prescriptions.

We explain our framework in Sec. II. Our results are shown in Sec. III. Section IV is devoted to a summary.

II. FRAMEWORK

Our framework is composed of GHFB and GFHB + AMP for structure and the Kyushu g-matrix DFM for reaction.

We determine the ground-state properties of Ca isotopes, using GHFB and GHFB + AMP [41]. In GHFB + AMP, the total wave function $|\Psi_M^I\rangle$ with the AMP is defined by

$$|\Psi_M^I\rangle = \sum_{K,n=1}^{N+1} g_{Kn}^I \hat{P}_{MK}^I |\Phi_n\rangle, \tag{1}$$

where $\hat{P}_{MK}^I$ is the angular momentum projector and the $|\Phi_n\rangle$ for $n = 1, 2, \ldots, N + 1$ are mean-field (GHFB) states, where N is the number of the states that one can block. The coefficients g_{Kn}^I are determined by solving the following Hill-Wheeler equation:

$$\sum_{K'n'} \mathcal{H}_{Kn,K'n'}^I g_{K'n'}^I = E_I \sum_{K'n'} \mathcal{N}_{Kn,K'n'}^I g_{K'n'}^I, \tag{2}$$

with the Hamiltonian and norm kernels defined by

$$\begin{Bmatrix} \mathcal{H}_{Kn,K'n'}^I \\ \mathcal{N}_{Kn,K'n'}^I \end{Bmatrix} = \langle \Phi_n | \begin{Bmatrix} \hat{H} \\ 1 \end{Bmatrix} \hat{P}_{KK'}^I | \Phi_{n'}\rangle. \tag{3}$$

For odd nuclei, we have to put a quasiparticle in a level, but the number N of the blocking states are quite large. It is not easy to solve the Hill-Wheeler equation with large N. Furthermore, we have to confirm that the resulting $|\Psi_M^I\rangle$ converges with respect to increasing N for any set of two deformations β and γ. This procedure is quite time-consuming. For this reason, we do not consider the AMP for odd nuclei. As for GHFB, we consider the one-quasiparticle state that yields the lowest energy, so that we do not have to solve the Hill-Wheeler equation. However, it is not easy to find the values of β and γ at which the energy becomes minimum in the β-γ plane.

For even nuclei, there is no blocking state, i.e., $N = 0$ in the Hill-Wheeler equation. We can thus consider GHFB + AMP. However, we have to find the value of β at which the ground-state energy becomes minimum. In this step, the AMP has to be performed for any β, so that the Hill-Wheeler calculation is still heavy. In fact, the AMP is not taken for most of the

TABLE I. Deformation parameters for Ca isotopes.

A	β^{AMP}	β	γ
40	0.093	0	
41		0.0320	-180
42	0.146	0	
43		0.00976	60
44	0.135	0	
45		0.0139	0.0599
46	0.137	0	
47		0.00908	-104
48	-0.116	0	
49		0.0239	60
50	0.121	0	
51		0.0199	8.94
52	-0.114	0	
53		0.00173	0.0631
54	0.130	0	
55		0.00195	-177
56	0.126	0	
57		0.000701	-180
58	-0.110	0	
59		0.0198	0.942
60	0.111	0	
62	0.131	0	
64	0.138	0	

mean-field calculations; see, for example, Ref. [44]. The reason we do not take into account γ deformation is that the deformation does not affect σ_R [20].

As a result of the heavy calculations for even nuclei, we find that β is small for GHFB + AMP. Meanwhile, the mean-field (GHFB) calculations yield that the energy surface becomes minimum at $\beta = 0$. The fact that $\beta = 0$ for GHFB and small for GHFB + AMP yields small difference between GHFB results and GHFB + AMP ones; see Table I for the values of β. In the table, we also show the values of β and γ for odd nuclei.

We predict σ_R for scattering of $^{40-60,62,64}$Ca on a ^{12}C target at $E_{\mathrm{lab}} = 280$ MeV, using the Kyushu g-matrix DFM [23]. In the DFM, the potential U between a projectile and a target is obtained by folding the Kyushu g-matrix with the projectile and target densities; see Eq. (9) of Ref. [23]. As for the densities, we adopt both GHFB and GHFB + AMP for even nuclei and GHFB for odd nuclei. As a way of making the center-of-mass correction, three methods were proposed in Refs. [10,20,45]. We used the method of Ref. [20], since the procedure is quite simple.

As already mentioned in Sec. I, the present folding model is successful in reproducing the differential cross sections of p scattering at $E_{\mathrm{lab}} = 65$ MeV [42] and of ^{4}He scattering at $E_{\mathrm{lab}} = 30$–200 MeV [23,43]. To show the reliability of the present DFB for σ_R, we apply the present DFM for the data on ^{12}C scattering on ^{9}Be, ^{12}C, and ^{27}Al targets in $30 \lesssim E_{\mathrm{lab}} \lesssim 400$ MeV and show that the present DFM is good in $30 \lesssim E_{\mathrm{lab}} \lesssim 100$ MeV and $250 \lesssim E_{\mathrm{lab}} \lesssim 400$ MeV. For light nuclei ^{9}Be, ^{12}C, ^{27}Al, we take the phenomenological

densities [38] deduced from the electron scattering; note that the phenomenological densities reproduce the experimental data [7] on r_m. For the densities of even Ca isotopes, we take GHFB with $\beta = 0$ and GHFB + AMP with β deformation in order to investigate effects of β deformation. As for the densities of odd Ca isotopes, we adopt GHFB in which β and γ deformations are taken into account.

III. RESULTS

Using GHFB and GHFB + AMP, we first determine the odd (even) dripline of Ca isotopes by seeing the values of S_1 (S_2) and find that ^{64}Ca is an even-dripline nucleus and ^{59}Ca is an odd-dripline nucleus. For $^{40-60,62,64}$Ca, we then present the ground-state properties (E_B, S_1, S_2, r_{ch}, r_p, r_n, r_m, r_{skin}, deformation). The theoretical results are consistent with the corresponding data. In the case that the experimental data are not available, we predict the the ground-state properties of $^{40-60,62,64}$Ca.

As stated in Sec. I, the Kyushu g-matrix folding model is successful in reproducing the differential cross sections of p scattering at $E_{\mathrm{lab}} = 65$ MeV [42] and of ^{4}He scattering at $E_{\mathrm{lab}} = 30$–200 MeV [23,43]. However, it is not clear whether the present DFM is reliable for σ_R. We then apply the present DFM for measured σ_R on ^{12}C scattering on ^{9}Be, ^{12}C, and ^{27}Al targets in $30 \lesssim E_{\mathrm{lab}} \lesssim 400$ MeV and show that the present DFM is reliable in $30 \lesssim E_{\mathrm{lab}} \lesssim 100$ MeV and $250 \lesssim E_{\mathrm{lab}} \lesssim 400$ MeV. After confirming the reliability of the Kyushu g-matrix DFM, we predict σ_R for scattering of $^{40-60,62,64}$Ca on a ^{12}C target at $E_{\mathrm{lab}} = 280$ MeV, since the data on σ_R will be available soon for $^{42-51}$Ca and the r_m are unknown for Ca isotopes except for ^{42,44,48}Ca. The prediction is made with the GHFB densities, since we confirm that effects of the AMP on σ_R are small.

A. Determination of even and odd driplines for Ca isotopes

We determine even and odd driplines, seeing A dependence of $S_1(A)$ and $S_2(A)$ and using the fact that nuclei are unbound for negative $S_1(A)$ and $S_2(A)$.

Figure 1 shows $S_1(A)$ and $S_2(A)$ as a function of A. The GHFB + AMP results are not plotted, since the results almost agree with the GHFB results. The GHFB results (open circles) are consistent with the data (crosses) on $S_1(A)$ and $S_2(A)$ [1–3]. Seeing A dependence of GHFB results, we can find that ^{64}Ca is an even-dripline nucleus and ^{59}Ca is an odd-dripline nucleus. The result is consistent with the observed line in Fig. 3 of Ref. [4].

B. Binding energies of Ca isotopes

Figure 2 shows $E_B(A)$ as a function of A from 40 to 64. The GHFB + AMP results are close to the GHFB ones (closed circles) for even Ca isotopes; in fact, the former deviates from the latter at most by 0.73%. For this reason, the GHFB + AMP results are not shown in Fig. 2. The GHFB results reproduce the experimental data (crosses) for $^{40-52}$Ca [1] and yield better agreement with the experimental data than coupled-cluster results (open circles) [29] based on NNLO$_{\mathrm{sat}}$.
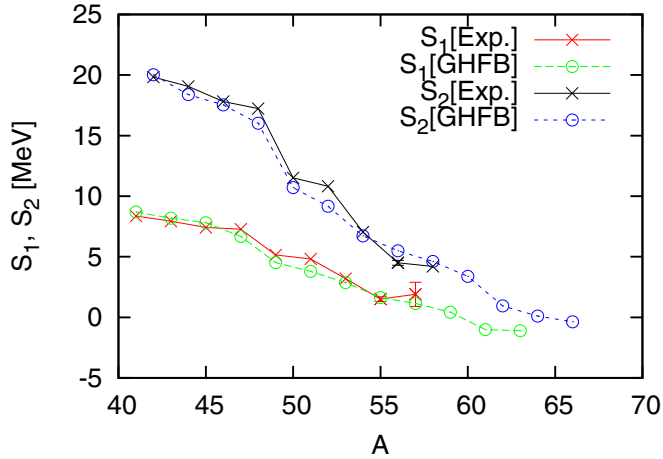
FIG. 1. *A* dependence of $S_1(A)$ and $S_2(A)$. Open circles show the GHFB results for S_1 and S_2. Experimental data (crosses) are taken from Refs. [1–3].
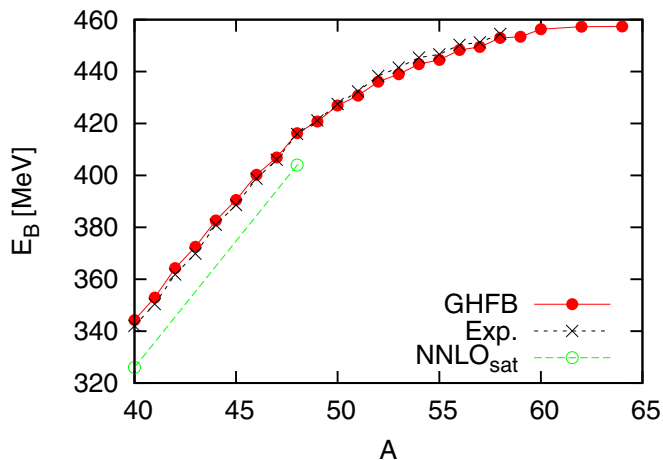

FIG. 3. *A* dependence of charge radii $r_{ch}(A)$. The GHFB results are shown by closed circles. Open circles denote the results [29] of coupled-cluster calculations based on NNLO$_{sat}$ for ^{40}Ca. Experimental data (crosses) are taken from Ref. [39].

C. Charge radii of Ca isotopes

Figure 3 shows r_{ch} as a function of A. The GHFB + AMP results agree with the GHFB ones for even Ca isotopes; in fact, the former deviates from the latter at most by 0.66%. For this reason, the GHFB + AMP results are not shown in Fig. 3. The GHFB results (closed circles) reproduce the experimental data (crosses) [39] derived from the isotope shift method based on the electron scattering for $^{40-52}$Ca; the former is deviated from the latter at most 0.9 %. For ^{40}Ca, the GHFB result agrees with the result [29] (open circle) of coupled-cluster calculations based on NNLO$_{sat}$.

D. Radii and skin of Ca isotopes

Figure 4 shows r_p, r_n, r_m, and r_{skin} as a function of A. The difference between GHFB + AMP (open circles) and GHFB

FIG. 2. *A* dependence of binding energy $E_B(A)$. The GHFB results are shown by closed circles. Open circles denote the results [29] of coupled-cluster calculations based on NNLO$_{sat}$. Experimental data (crosses) are taken from the homepage NuDat 2.7 [1].
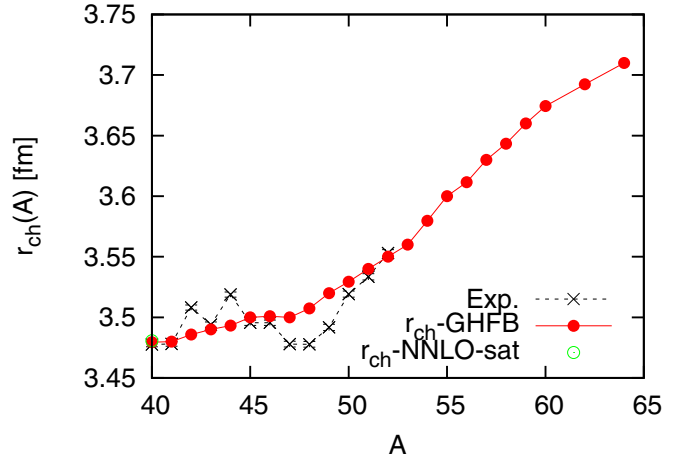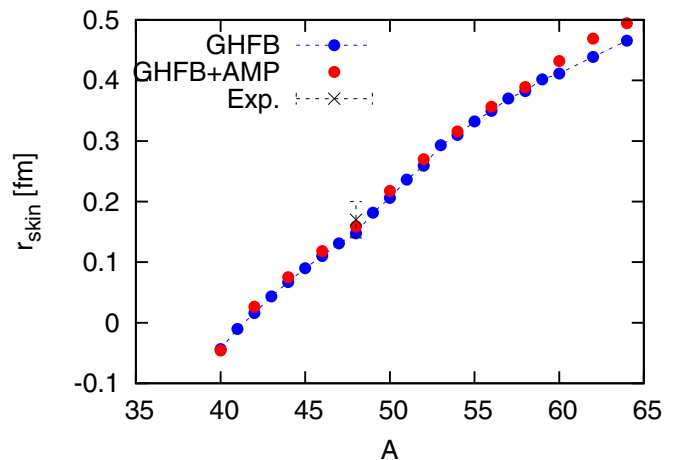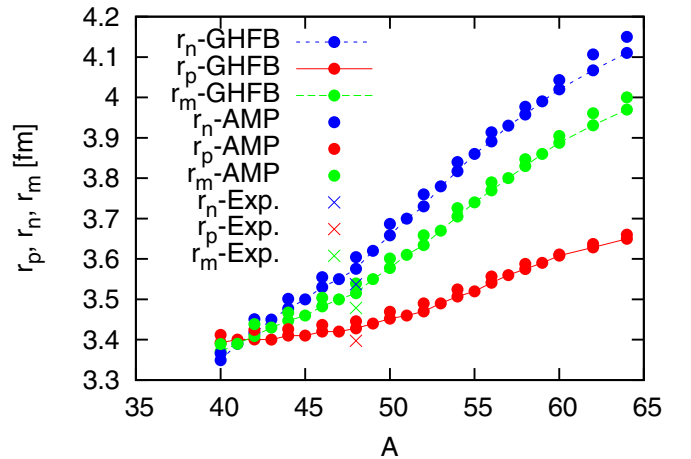
FIG. 4. *A* dependence of r_p, r_n, and r_m in the upper panel and r_{skin} in the lower panel. Tangent lines with closed circles denote the GHFB results, while closed circles correspond to the GHFB+AMP results. Experimental data (crosses) are taken from Ref. [37].

TABLE II. Radii for Ca isotopes. The superscript "AMP" stands for the results of GHFB+AMP, and no superscript corresponds to those of GHFB.

A	r_n^{AMP}	r_p^{AMP}	r_m^{AMP}	$r_{\mathrm{skin}}^{\mathrm{AMP}}$	r_n	r_p	r_m	r_{skin}
40	3.366	3.412	3.389	−0.046	3.349	3.393	3.371	
41					3.387	3.397	3.392	−0.010
42	3.451	3.424	3.438	0.026	3.417	3.401	3.409	
43					3.448	3.405	3.428	0.043
44	3.501	3.426	3.467	0.075	3.477	3.410	3.447	
45					3.504	3.414	3.465	0.090
46	3.555	3.436	3.504	0.118	3.530	3.420	3.483	
47					3.554	3.424	3.499	0.131
48	3.604	3.445	3.539	0.159	3.576	3.428	3.515	
49					3.621	3.440	3.548	0.182
50	3.687	3.469	3.601	0.218	3.658	3.452	3.577	
51					3.698	3.462	3.607	0.236
52	3.760	3.490	3.659	0.270	3.734	3.475	3.577	
53					3.779	3.486	3.671	0.293
54	3.840	3.524	3.726	0.316	3.817	3.507	3.705	
55					3.856	3.524	3.739	0.332
56	3.913	3.557	3.790	0.357	3.891	3.541	3.770	
57					3.928	3.557	3.802	0.370
58	3.977	3.588	3.847	0.389	3.958	3.575	3.830	
59					3.995	3.593	3.863	0.402
60	4.043	3.611	3.904	0.432	4.020	3.608	3.888	
62	4.106	3.637	3.961	0.469	4.067	3.628	3.931	
64	4.153	3.658	4.005	0.494	4.113	3.648	3.974	

(closed circles) is small for even Ca isotopes; in fact, the former deviates from the latter at most by 0.8% for r_m. The reason for the small difference is that β is small for GHFB + AMP and zero for GHFB, as shown in Table I. Particularly for ^{48}Ca, the experimental data are available [37]. The deviation of the GHFB + AMP result from the data (crosses) and is 1.1% for r_m. This indicates that the GHFB + AMP and GFHB are good enough for explaining the data. Our results on radii and skin are tabulated in Table II.

E. Prediction on σ_R for $^{40-60,62,64}$Ca + ^{12}C scattering at $E_{\mathrm{lab}} = 280$ MeV

At first, we confirm the reliability of the present DFM for σ_R at $E_{\mathrm{lab}} = 280$ MeV, as seen in Fig. 5. The DFM results (open circles) reproduce the experimental data (crosses) [7] for ^{9}Be, ^{12}C, and ^{27}Al. Also for ^{40}Ca, good agreement is seen between the DFM result with GHFB + AMP density (open circle) and the experimental data (cross); note that $E_{\mathrm{lab}} = 250.7$ MeV for the data [12].

Figure 6 is our prediction on σ_R for $^{40-60,62,64}$Ca at $E_{\mathrm{lab}} = 280$ MeV. For ^{40}Ca, the DFM results with GHFB and GHFB + AMP densities (open and closed circles) agree with the experimental data [12] at $E_{\mathrm{lab}} = 250.7$ MeV. The difference between the GHFB and GHFB + AMP densities is small. This comes from the fact that for even Ca isotopes the β are zero for GHFB and small for GHFB + AMP; see Table I for the values of β.
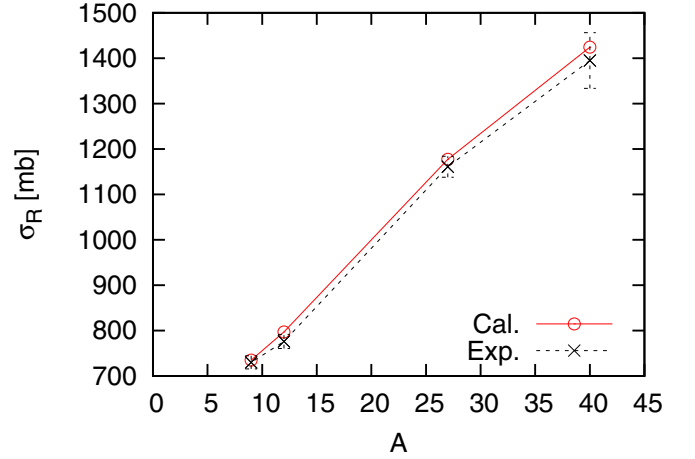

FIG. 5. Reaction cross sections σ_R for ^{12}C scattering on ^{9}Be, ^{12}C, ^{27}Al, and ^{40}Ca targets at $E_n = 280$ MeV. Open circles denote the DFM results. The experimental data (crosses) are taken from Ref. [7] for ^{9}Be, ^{12}C, and ^{27}Al and Ref. [12] for ^{40}Ca; note that $E_{\mathrm{lab}} = 250.7$ MeV for ^{40}Ca.

F. Reaction cross sections in $30 \lesssim E_{\mathrm{lab}} \lesssim 400$ MeV

Through the analyses in Secs. III C–III E, we can conclude that the σ_R calculated with the Kyushu *g*-matrix DFM is valid for $^{40-60,62,64}$Ca + ^{12}C scattering at $E_{\mathrm{lab}} = 280$ MeV. We then investigate how reliable the present DFM is for a wide range of E_{lab}. For this purpose, we consider ^{12}C scattering on ^{9}Be, ^{12}C, and ^{27}Al targets in $30 \lesssim E_{\mathrm{lab}} \lesssim 400$ MeV, since high-quality data are available [7].

Figure 7 shows σ_R as a function of E_{lab} for ^{12}C + ^{12}C scattering. Comparing our results with the data [7], we confirm that the present DFM is reliable in $30 \lesssim E_{\mathrm{lab}} \lesssim 100$ MeV and $250 \lesssim E_{\mathrm{lab}} \lesssim 400$ MeV. The *g*-matrix DFM results (closed squares) yield much better agreement with the experimental
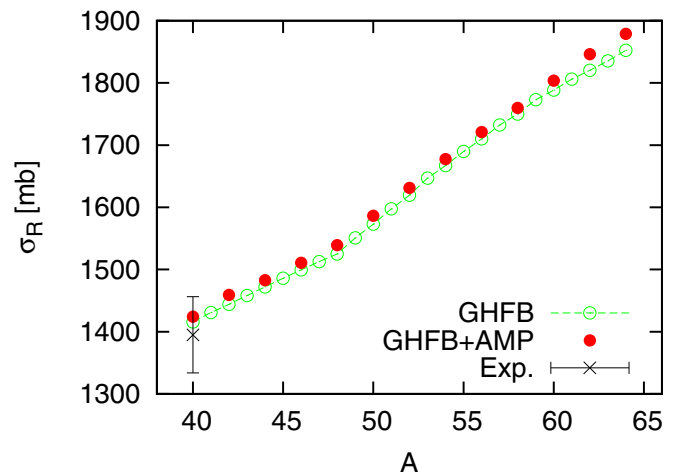

FIG. 6. *A* dependence of σ_R on $^{40-60,62,64}$Ca on a ^{12}C target at $E_{\mathrm{lab}} = 280$ MeV. The DFM results with GHFB and GHFB + AMP densities are shown by open and closed circles, respectively. The experimental data [12] for ^{40}Ca + ^{12}C scattering at $E_{\mathrm{lab}} = 250.7$ MeV is denoted by a cross with error bar.
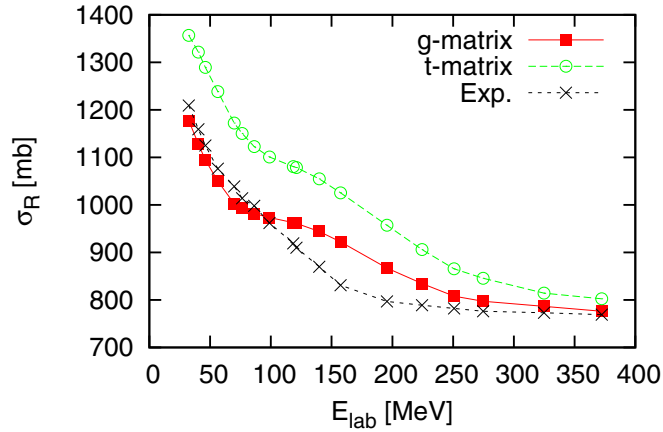
FIG. 7. E_{lab} dependence of σ_R for ^{12}C + ^{12}C scattering. Closed squares denote the *g*-matrix DFM results, while open circles correspond to the *t*-matrix DFM results densities. The experimental data (crosses) are taken from Ref. [7].

data (crosses) than the *t*-matrix DFM results (open circles) do; note that only the Kyushu and the Melbourne *g* matrix approach the *t* matrix, as ρ becomes zero. At $E_{lab} = 380$ MeV, the *t*-matrix DFM result overestimates the data only by 4%, so that we may consider that the *t*-matrix DFM is accurate enough for ^{12}C + ^{12}C scattering in $E_{lab} \gtrsim 400$ MeV.

Figure 8 shows E_{lab} dependence of $f(E_{lab}) \equiv \sigma_R^{exp}(C + C)/\sigma_R^{th}(C + C)$ for ^{12}C + ^{12}C scattering, where σ_R^{th} is the *g*-matrix DFM result. The factor $|1 - f|$ means an error of the present DFM and becomes maximum around $E_{lab} = 160$ MeV. Since the maximum error is still small, we guess that it comes from higher-order terms of chiral expansion for bare nucleon-nucleon force. Further explanation will be shown in Sec. IV.

In order to minimize the error for other systems, we multiply "σ_R^{th}(other system) calculated with the *g*-matrix DFM" by the factor $f(E_{lab})$ and call the result "the renormalized *g*-matrix DFM result" from now on.
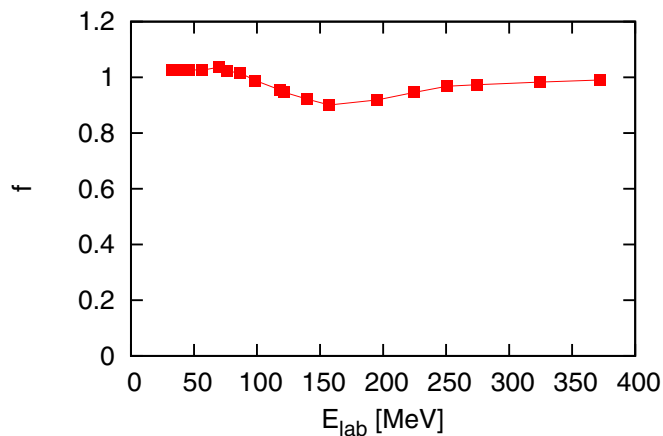

FIG. 8. E_{lab} dependence of f for ^{12}C + ^{12}C scattering. Closed squares stand for $f(E_{lab}) \equiv \sigma_R^{exp}(C + C)/\sigma_R^{th}(C + C)$.
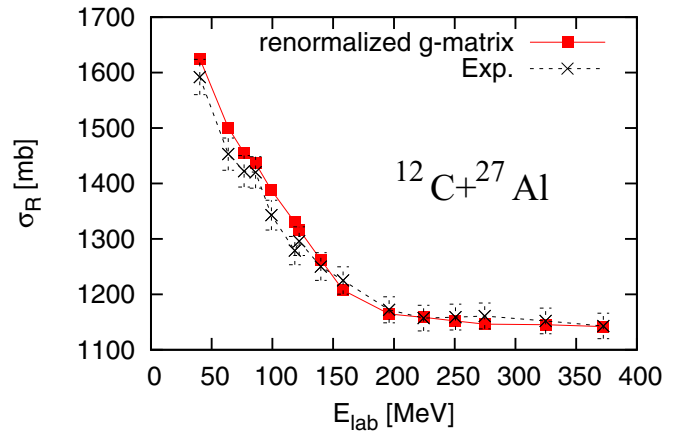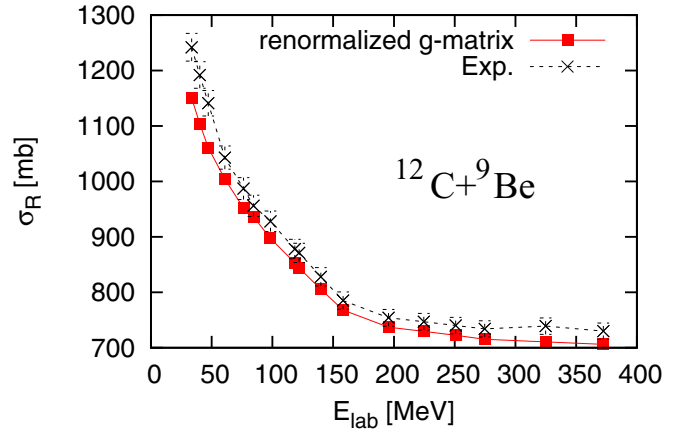

FIG. 9. E_{lab} dependence of σ_R for ^{12}C scattering on ^{7}Be and ^{27}Al targets. Closed squares show the renormalized *g*-matrix DFM results. The experimental data (crosses) are taken from Ref. [7].

Figure 9 shows E_{lab} dependence of σ_R for ^{12}C scattering on ^{9}Be and ^{27}Al targets. The renormalized *g*-matrix DFM results (closed squares) agree with the experimental data (crosses) [7] within experimental error for $E_{lab} \gtrsim 75$ MeV. The renormalized *g*-matrix DFM results are reliable for $E_{lab} \gtrsim 75$ MeV.

As an alternative prescription to the renormalized *g*-matrix DFM, we fit the imaginary part of the potential (*g* matrix) to the data on σ_R for ^{12}C - ^{12}C scattering. The fitting factor f_w is shown in Fig. 10. The f_w tends to 1 as E_{lab} increases. Figure 11 shows the results of DFM with the fitted *g* matrix for ^{12}C scattering on a ^{9}Be target. The fitted DFM well reproduces the data in $E_{lab} \gtrsim 300$ MeV. For the other E_{lab}, the fitted DFM overestimates the data at most 13%.

IV. SUMMARY

We predicted the ground-state properties of Ca isotopes using GHFB and GHFB + AMP, and predicted the σ_R for scattering of Ca isotopes on a ^{12}C target at $E_{lab} = 280$ MeV by using the Kyushu *g*-matrix DFM [23]. Details of the predictions are shown below.

As an important property of Ca isotopes, we first determined the odd and even driplines by seeing A dependence of S_1 and S_2 and found that ^{64}Ca is an even-dripline nucleus
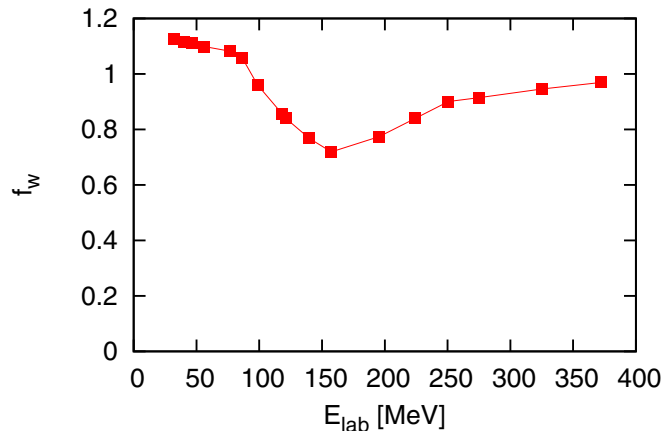
FIG. 10. E_{lab} dependence of f_w for $^{12}\text{C} + ^{12}\text{C}$ scattering. Closed squares stand for f_w.

FIG. 11. E_{lab} dependence of σ_R for ^{12}C scattering on ^9Be target. Closed squares show the fitted *g*-matrix DFM results. The experimental data (crosses) are taken from Ref. [7].

and ^{59}Ca is an odd-dripline nucleus. As for E_B in addition to S_1, S_2, our results agree with the experimental data [1–4] in $^{40-58}\text{Ca}$. Our results are thus accurate enough for the prediction on the odd and even driplines.

As other grand-state properties of Ca isotopes, we considered r_{ch}, r_p, r_n, r_m, r_{skin}, deformation for $^{40-60,62,64}\text{Ca}$. For $^{40-52}\text{Ca}$, the r_{ch} calculated with GHFB and GHFB + AMP are consistent with those [39] deduced from the isotope shift method based on the electron scattering. As for r_p, r_n, r_m, and r_{skin}, the experimental data are available for ^{48}Ca [37], and our results agree with the data. The success mentioned above for the ground-state properties indicates that the densities calculated with GHFB and GHFB + AMP are reliable for Ca isotopes.

The Kyushu *g*-matrix folding model is successful in reproducing the differential cross sections of *p* scattering at $E_{lab} =$ 65 MeV [42] and of ^4He scattering at $E_{lab} =$ 30–200 MeV [23,43]. However, it is not clear whether the Kyushu *g*-matrix DFM is reliable for σ_R. We then applied the Kyushu *g*-matrix DFM for measured σ_R on ^{12}C scattering from ^9Be, ^{12}C, and ^{27}Al targets in $30 \lesssim E_{lab} \lesssim 400$ MeV and confirmed that the Kyushu *g*-matrix DFM is reliable in $30 \lesssim E_{lab} \lesssim 100$ MeV and $250 \lesssim E_{lab} \lesssim 400$ MeV. We then predict σ_R for scattering of Ca isotopes on a ^{12}C target at $E_{lab} = 280$ MeV, using the
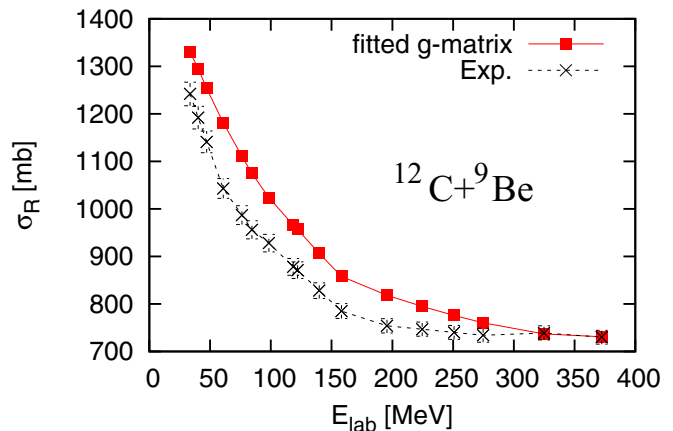
Kyushu *g*-matrix DFM. The reason for this prediction is that (1) the data on σ_R for $^{42-51}\text{Ca}$ will be available soon and (2) the densities are determined accurately for Ca isotopes.

The present DFM is not accurate enough for ^{12}C - ^{12}C scattering in $110 \lesssim E_{lab} \lesssim 240$ MeV. Whenever we use the chiral interaction, E_{lab} should be smaller than $\Lambda = 550$ MeV. In general, the chiral *g*-matrix DFM becomes less accurate as E_{lab} increases. The small error in $110 \lesssim E_{lab} \lesssim 240$ MeV seems to come from terms higher than the present order. The reason why the present DFM is good for higher E_{lab} is that the present *g* matrix approaches the *t* matrix as E_{lab} increases. In order to improve the present DFM in $110 \lesssim E_{lab} \lesssim 240$ MeV, we have proposed two prescriptions. The renormalized DFM proposed is good for $30 \lesssim E_{lab} \lesssim 400$ MeV. The values of the present *g* matrix is published in Ref. [23] and the homepage http://www.nt.phys.kyushu-u.ac.jp/english/gmatrix.html. For $E_{lab} \gtrsim 400$ MeV, we recommend the *t*-matrix DFM.

[1] The National Nuclear Data Center, NuDat 2.7 [https://nucleus.iaea.org/Pages/nu-dat-2.aspx].

[2] O. B. Tarasov *et al.*, Phys. Rev. Lett. **121**, 022501 (2018).

[3] S. Michimasa *et al.*, Phys. Rev. Lett. **121**, 022506 (2018).

[4] L. Neufcourt, Y. Cao, W. Nazarewicz, E. Olsen, and F. Viens, Phys. Rev. Lett. **122**, 062502 (2019).

[5] I. Tanihata, H. Hamagaki, O. Hashimoto, Y. Shida, N. Yoshikawa, K. Sugimoto, O. Yamakawa, T. Kobayashi, and N. Takahashi, Phys. Rev. Lett. **55**, 2676 (1985).

[6] J. S. Al-Khalili and J. A. Tostevin, Phys. Rev. Lett. **76**, 3903 (1996).

[7] M. Takechi, M. Fukuda, M. Mihara, K. Tanaka, T. Chinda, T. Matsumasa, M. Nishimoto, R. Matsumiya, Y. Nakashima,

H. Matsubara, K. Matsuta, T. Minamisono, T. Ohtsubo, T. Izumikawa, S. Momota, T. Suzuki, T. Yamaguchi, R. Koyama, W. Shinozaki, M. Takahashi, A. Takizawa, T. Matsuyama, S. Nakajima, K. Kobayashi, M. Hosoi, T. Suda, M. Sasaki, S. Sato, M. Kanazawa, and A. Kitagawa, Phys. Rev. C **79**, 061601(R) (2009).

[8] M. Takechi *et al.*, Phys. Lett. B **707**, 357 (2012).

[9] R. Kanungo *et al.*, Phys. Rev. Lett. **117**, 102501 (2016).

[10] W. Horiuchi, Y. Suzuki, B. Abu-Ibrahim, and A. Kohama, Phys. Rev. C **75**, 044607 (2007); **76**, 039903(E) (2007)].

[11] Y. Togano *et al.*, Phys. Lett. B **761**, 412 (2016).

[12] M. Takechi *et al.*, Phys. Rev. C **90**, 061305 (2014).

[13] M. Yahiro, S. Watanabe, M. Toyokawa and T. Matsumoto, Phys. Rev. C **93**, 064609 (2016).

[14] M. Tanaka *et al.*, arXiv:1911.05262 [nucl-ex].

[15] M. Yahiro, K. Minomo, K. Ogata, and M. Kawai, Prog. Theor. Phys. **120**, 767 (2008).

[16] F. A. Brieva and J. R. Rook, Nucl. Phys. A **291**, 299 (1977); **291**, 317 (1977); **297**, 206 (1978).

[17] K. Amos, P. J. Dortmans, H. V. von Geramb, S. Karataglidis, and J. Raynal, in *Advances in Nuclear Physics*, Vol. 25, edited by J. W. Negele and E. Vogt (Plenum, New York, 2000), p. 275.

[18] T. Furumoto, Y. Sakuragi, and Y. Yamamoto, Phys. Rev. C **78**, 044610 (2008).

[19] K. Minomo, T. Sumi, M. Kimura, K. Ogata, Y. R. Shimizu, and M. Yahiro, Phys. Rev. Lett. **108**, 052503 (2012).

[20] T. Sumi, K. Minomo, S. Tagami, M. Kimura, T. Matsumoto, K. Ogata, Y. R. Shimizu, and M. Yahiro, Phys. Rev. C **85**, 064613 (2012).

[21] K. Egashira, K. Minomo, M. Toyokawa, T. Matsumoto, and M. Yahiro, Phys. Rev. C **89**, 064611 (2014).

[22] S. Watanabe *et al.*, Phys. Rev. C **89**, 044610 (2014).

[23] M. Toyokawa, M. Yahiro, T. Matsumoto, and M. Kohno, PTEP **2018**, 023D03 (2018). See http://www.nt.phys.kyushu-u.ac.jp/english/gmatrix.html for Kyushu *g*-matrix.

[24] M. Kohno, Phys. Rev. C **88**, 064005 (2013).

[25] M. Kohno, Phys. Rev. C **96**, 059903(E) (2017).

[26] H. V. von Geramb, K. Amos, L. Berge, S. Bräutigam, H. Kohlhoff, and A. Ingemarsson, Phys. Rev. C **44**, 73 (1991).

[27] P. J. Dortmans and K. Amos, Phys. Rev. C **49**, 1309 (1994).

[28] G. Hagen, T. Papenbrock, M. Hjorth-Jensen and D. J. Dean, Rept. Prog. Phys. **77**, 096302 (2014).

[29] G. Hagen *et al.*, Nat. Phys. **12**, 186 (2015).

[30] S. Weinberg, Nucl. Phys. B **363**, 3 (1991).

[31] E. Epelbaum, H. W. Hammer, and Ulf-G. Meissner, Rev. Mod. Phys. **81**, 1773 (2009).

[32] R. Machleidt and D. R. Entem, Phys. Rept. **503**, 1 (2011).

[33] A. Ekstrom, G. R. Jansen, K. A. Wendt, G. Hagen, T. Papenbrock, B. D. Carlsson, C. Forssen, M. Hjorth-Jensen, P. Navratil, and W. Nazarewicz, Phys. Rev. C **91**, 051301(R) (2015).

[34] R. F. Garcia Ruiz *et al.*, Nat. Phys. **12**, 594 (2016).

[35] K. Hebeler, S. K. Bogner, R. J. Furnstahl, A. Nogga, and A. Schwenk, Phys. Rev. C **83**, 031301(R) (2011).

[36] R. J. Furnstahl and K. Hebeler, Rept. Prog. Phys. **76**, 126301 (2013).

[37] J. Birkhan *et al.*, Phys. Rev. Lett. **118**, 252501 (2017).

[38] H. de Vries, C. W. de Jager, and C. de Vries, At. Data Nucl. Data Tables **36**, 495 (1987).

[39] I. Angeli and K. P. Marinova, At. Data Nucl. Data Tables **99**, 69 (2013).

[40] A. Ong, J. C. Berengut, and V. V. Flambaum, Phys. Rev. C **82**, 014320 (2010).

[41] S. Tagami, Y. R. Shimizu, and J. Dudek, J. Phys. G **42**, 015106 (2015).

[42] M. Toyokawa, K. Minomo, M. Kohno and M. Yahiro, J. Phys. G **42**, 025104 (2015); **44**, 079502 (2017).

[43] M. Toyokawa, M. Yahiro, T. Matsumoto, K. Minomo, K. Ogata and M. Kohno, Phys. Rev. C **92**, 024618 (2015); **96**, 059905 (2017).

[44] S. Hilaire and M. Girod, Hartree-Fock-Bogoliubov results based on the Gogny force [http://www-phynu.cea.fr/science-en-ligne/carte-potentiels-microscopiques/carte-potentiel-nucleaire-eng.htm].

[45] L. J. Tassie and F. C. Barker, Phys. Rev. **111**, 940 (1958).